frontiers | Frontiers in Earth Science

TYPE Original Research
PUBLISHED 27 November 2024
DOI 10.3389/feart.2024.1478570

OPEN ACCESS

EDITED BY
Faming Huang,
Nanchang University, China

REVIEWED BY
Chong Xu,
Ministry of Emergency Management, China
P. V. Divya,
Indian Institute of Technology Palakkad, India

*CORRESPONDENCE
Hao Man,
manhao6628052@qq.com

RECEIVED 10 August 2024
ACCEPTED 14 November 2024
PUBLISHED 27 November 2024

CITATION
Gu C, Chen L, Zuo W, Li W, Man H, Lu H and Ji F (2024) Study on rainfall infiltration characteristics and instability mechanism of a lateritic soil landslide in Yunnan, China. *Front. Earth Sci.* 12:1478570. doi: 10.3389/feart.2024.1478570

Study on rainfall infiltration characteristics and instability mechanism of a lateritic soil landslide in Yunnan, China

Chuan Gu[1], Liang Chen[1], Weizhong Zuo[1], Weile Li[2], Hao Man[2]*, Hanyu Lu[2] and Feng Ji[2]

[1]Liangshan Mining Co., Ltd., Huili Sichuan, China, [2]State Key Laboratory of Geohazard Prevention and Geoenvironment Protection, Chengdu University of Technology, Chengdu, China

Introduction: The engineering geological characteristics of Yunnan's lateritic soil are quite unique, making it prone to shallow group landslides under rainfall conditions. This study focused on an old lateritic soil landslide as a case study.

Methods: Soil column ponding infiltration experiment was conducted to investigate the infiltration behavior of the lateritic soil. Numerical simulation software was employed to analyze the rainfall-induced seepage characteristics of the landslide, and a comprehensive assessment of the failure mechanisms of the lateritic soil landslide was conducted.

Results: The study findings are as follows: (1) During water infiltration, the infiltration time curve of the lateritic soil column showed a parabolic growth trend. The migration rate of the wetting front rapidly decreased from 0.15 to 0.2 cm/min to 0.1 cm/min and then stabilized at approximately 0.04 cm/min. (2) Long-term heavy rainfall is the condition for the formation of this old lateritic soil landslide. By coupling the seepage process, the stability coefficient of the lateritic soil slope was calculated, revealing that the instability rainfall threshold of the slope under prolonged rainfall conditions is generally 120 mm/d. (3) The main changes in the seepage field occurred in the shallow soil layer. In the later stages of rainfall, the infiltration rate of the slope was controlled by the permeability coefficient of the lateritic soil. As the rainfall intensity increased, the depth of rainfall impact increased, and the pore water pressure in the shallow soil layer tended to gradually increase and then stabilize under different rainfall intensities. (4) Under long-term rainfall conditions, the volumetric water content of the soil at the toe of the lateritic soil slope first peaked. After the rainfall ended, moisture in the slope continued to migrate to the toe, keeping the soil at the toe in a saturated state. (5) The formation and evolution of this lateritic soil landslide could be divided into five stages: initial natural stage, rainfall infiltration-crack expansion, shallow creep-progressive collapse of the front edge, sliding surface penetration-overall instability, and landslide braking accumulation.

Conclusion: The research results provide significant theoretical guidance and practical implications for understanding the causes and prevention of lateritic soil landslides in similar areas.

KEYWORDS

lateritic soil, landslide, rainfall infiltration, instability threshold, failure evolution

Introduction

Lateritic soil is residual soil formed from iron-bearing parent rock through lateritization in a hot and humid climate and is widely distributed in the southwestern region of China (Fu et al., 1997; Chantruthai et al., 2017; Sani and Eisazadeh, 2023). The surface layer of lateritic soil on slopes is relatively dry, loose, and of low strength, making it susceptible to water erosion. The deeper the soil is, the greater the strength and density. The instability of slopes composed of lateritic soil is closely related to rainfall.

Under natural conditions, slopes are generally in an unsaturated state, and rainfall is the most significant external dynamic factor affecting slope stability. Rainwater infiltration can lead to changes in internal stress within slopes, potentially causing slope instability (Fourie et al., 1999; Ye et al., 2015; Froude and Petley, 2018; Tao et al., 2024). Researchers have conducted extensive studies on the seepage characteristics and stability variations of unsaturated soil slopes under rainfall conditions via physical model experiments (Chen, 2014; Song et al., 2021; Lu et al., 2023) and numerical simulation methods (Zeng et al., 2017; Wang et al., 2019; Yuan et al., 2020; Xu et al., 2022; Li et al., 2021).

For example, Zhou et al. (2023) conducted an analysis via Geo-studio software to study the characteristics of pore water pressure variation within unsaturated soil slopes and the impact of different rainfall conditions on slope stability. Tran et al. (2018) developed a slope model based on instantaneous rainfall infiltration to analyze the dynamic changes in the seepage field within a slope and the corresponding stability variations. Cheng et al. (2024) proposed a rigorous limit equilibrium method and, using SEEP/W software in conjunction with this method, investigated the effects of rainfall intensity, rainfall pattern, and duration on soil slope stability. Bai et al. (2023) conducted a field rainfall experiment on a natural double-layer loess slope, combined with finite element software simulations to analyze the rainfall infiltration characteristics of the slope and the infiltration effects at the soil layer interface. The results indicated that as the rainfall intensity increased, the infiltration effects at the interface became more pronounced.

When the rainfall volume and intensity exceed critical thresholds, geological hazards may occur in clusters (Sun et al., 2022). Many researchers have proposed reasonable rainfall thresholds for triggering landslide instability by considering various influencing factors on the basis of hydrological and landslide stability models (Liu et al., 2023; Gong et al., 2024; Bhavithra et al., 2024; Sun et al., 2024). Both short-term intense rainfall and long-term continuous rainfall can potentially lead to slope instability (Fu et al., 2012; Shi et al., 2016; Ma et al., 2021; Hou et al., 2021). Cui et al. (2007) utilized numerical methods to investigate the failure process of a highway slope under prolonged continuous rainfall conditions. The results indicated that the loss of soil suction caused by rainfall was the primary factor leading to slope failure. Zheng et al. (2016) developed a finite element model for gravel soil slopes to analyze the seepage process and stability under prolonged heavy rainfall. Li et al. (2023b) conducted physical model experiments and numerical simulations on layered soil slopes under heavy rainfall. The results showed that infiltration under heavy rainfall primarily occurred in the shallow layers of the slope. The rainfall increased pore water pressure, thereby weakening the shear strength of the soil. Liu et al. (2012) analyzed the changes in soil moisture content and shear strength during the infiltration process under continuous low-intensity rainfall. Using FLAC3D, they studied the dynamic changes in the slope safety factor. The results indicated that during continuous low-intensity rainfall, the critical sliding surface of the slope had not yet become saturated.

In summary, considerable research has been conducted on the rainfall infiltration process and slope stability of unsaturated soils, with most studies focusing on the effects of rainfall intensity and duration on the stability of unsaturated slopes. However, lateritic soils, which exhibit high shrinkage and unique engineering geological characteristics, have been less studied in terms of their seepage properties and slope stability. To address this gap, this study focused on an old lateritic landslide in Yunnan Province. On the basis of field investigations, laboratory tests, and an analysis of local rainfall characteristics, the rainfall-induced seepage behavior and instability thresholds of the lateritic slope were examined. The findings provide valuable theoretical insights and practical implications for understanding the causes of lateritic landslides and mitigating geological hazards in similar regions.

Geological characteristics of the landslide

The lateritic soil landslide in the study area is an old landslide with a long, tongue-shaped platform and a main sliding direction of 94°. The landslide site is located on the eastern side of the central Hengduan Mountains and the northern edge of the Yunnan Plateau, with geographic coordinates of N26°11′15.45″, E101°57′38.23″. The landslide is 480–500 m long and approximately 200–400 m wide, with a height difference of 117–120 m between the leading and rear edges. The landslide boundaries are distinct, with a steep, chair-shaped landslide back wall at the rear edge, approximately 32 m in height. After slope instability, a pull-down trench formed at the rear of the slope and was filled with gravel soil. The boundaries on both sides are steep, nearly vertical walls (Figure 1).

During its formation, the landslide developed multiple terraces. The quartz albite schist is exposed at the front edge. Currently, most landslide masses have been converted into agricultural land by local residents. According to field geological investigations, the slope is steeper in the middle and front sections, whereas the middle to rear sections form a terrace. The steep front and gentle rear topography provided favorable conditions for landslide development. The gentle slope has an open surface, which prolongs surface water retention, facilitating rainfall infiltration. A stream runs along the front edge of the slope, with a significant increase in flow during the rainy season. Continuous scouring and erosion of the opposite bank weaken the soil strength at the front, causing the front soil to become unstable and be carried away by the water flow. This process continuously pulls the rear soil, ultimately leading to the formation of the landslide. The longitudinal profile of the main sliding direction is shown in Figure 2.

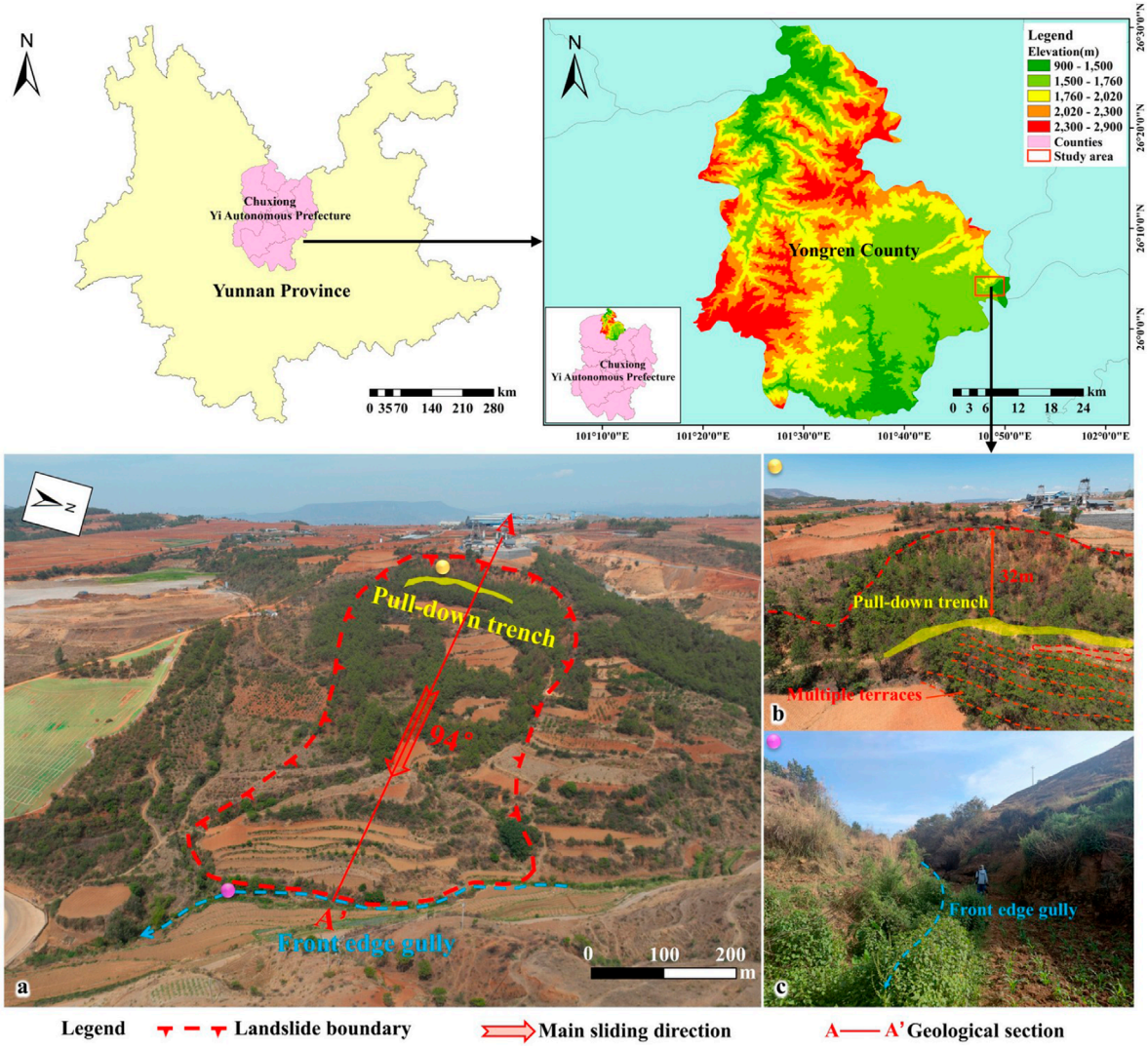

FIGURE 1
Landslide overview (**A**). Overall view of the landslide; (**B**). Rear edge of the landslide; (**C**). Front edge of the landslide).

One-dimensional soil column infiltration test

Test equipment and sensor installation

The soil samples used in the soil column experiment were collected from the middle front and the left side of the landslide body, where vegetation cover is sparse. Disturbed soil samples were obtained by first using shovels and picks to remove approximately 10 cm of the surface layer, which had been significantly influenced by external factors. Large boulders with excessive particle sizes were discarded during the process. A sampling pit with a depth of 50 cm was then excavated for sample collection.

The one-dimensional soil column infiltration test equipment consists primarily of a cylindrical tube containing the lateritic soil sample, a data acquisition system, sensors, a water supply device, and imaging equipment. The cylindrical tube is made of acrylic material, with a height of 100 cm and inner and outer diameters of 25 cm and 27 cm, respectively. The top of the tube was opened, and the bottom was sealed, with a 2 cm diameter drainage outlet near the base. Six volumetric water content sensors and three matric suction sensors were embedded in the soil column at different depths from top to bottom (Figure 3). The water supply device consists of a medical-grade infusion bottle and drip line, with the flow rate controlled by adjusting the air pressure. A water pump was used to quickly fill the space above the soil sample to a water head height of 10 cm for a constant head ponded infiltration test. During the infiltration process, a sufficient water supply was maintained to ensure a stable water head.

Analysis of test results

The data collected by the sensors were used to plot the variation curves of the volumetric water content of the lateritic soil over time and depth (Figures 4, 5). As shown in the figures, the initial

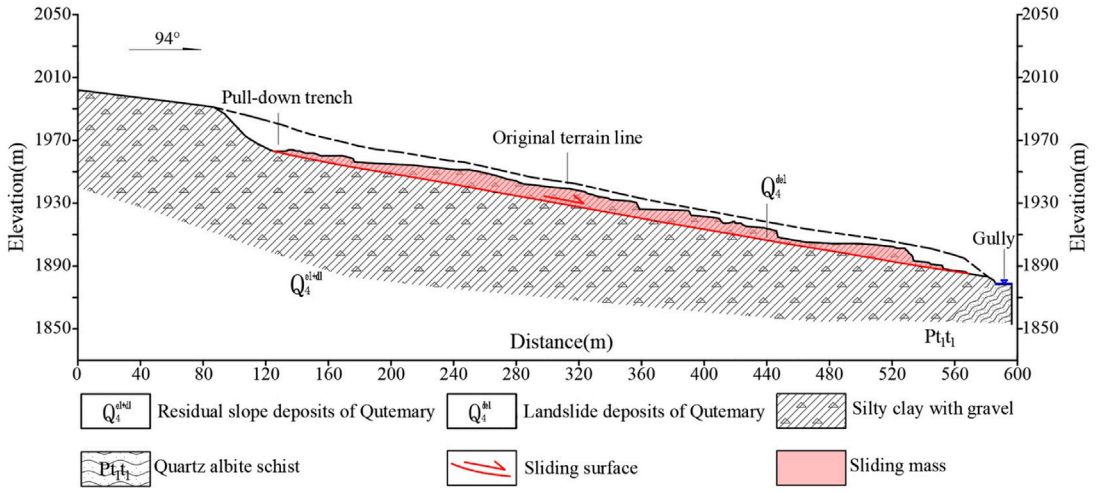

FIGURE 2
The main sliding direction profile of the landslide.

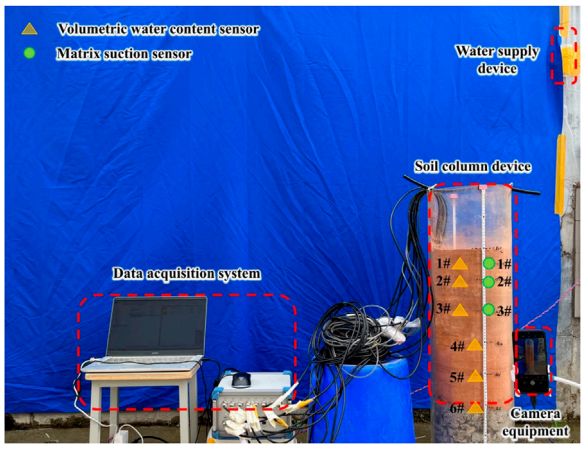

FIGURE 3
Soil column test equipment.

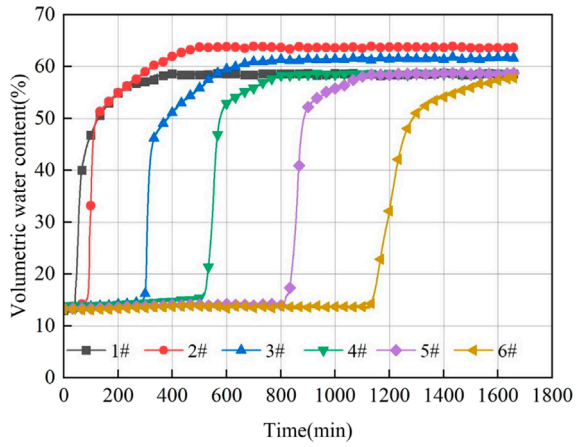

FIGURE 4
Time-variation curve of the volumetric water content.

volumetric water content at different depths varied slightly, ranging between 10% and 15%. As rainfall slowly infiltrated, the sensors responded sequentially, with the volumetric water content first increasing sharply and then rising more gradually until stabilizing. The changes in water content were more pronounced in the shallow soil than in the deeper soil. Once the soil above the wetting front became saturated, water movement was no longer driven by the matric potential, resulting in a decrease in the infiltration rate. As the wetting front moved downward, the moisture at the leading edge was not replenished in time. The rate of increase in the volumetric water content recorded by each sensor gradually decreased with increasing sensor burial depth.

Figure 6 shows the time series curve of matric suction in the lateritic soil. In the initial state, the soil was dry, and the initial matric suction at the sensor locations was close to 700 kPa, representing the maximum value. The response pattern of matric suction was opposite to that of the volumetric water content. As the soil gradually saturated with water infiltration, the matric suction decreased sharply as water passed through the sensors, decreasing to a minimum value of approximately 10 kPa within a short period. The matric suction subsequently remained unchanged despite further water infiltration.

Figure 7 presents the time series curves of the wetting front migration depth and migration velocity in the lateritic soil. The migration depth curve shows a parabolic growth trend, with the infiltration depth decreasing gradually over time at the same infiltration duration. The distance advanced by the wetting front per unit time represents the migration velocity of the wetting front. In the early stage of infiltration, the wetting front migration velocity decreased significantly, dropping rapidly from the initial maximum

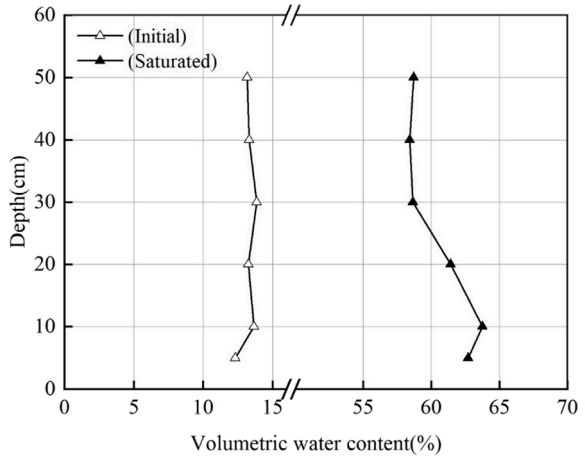

FIGURE 5
Depth-variation curve of the volumetric water content.

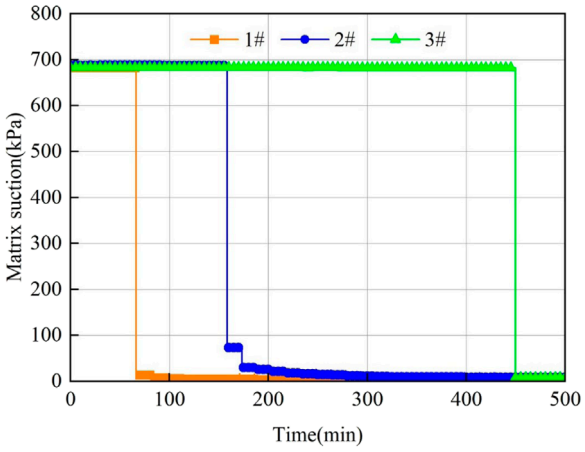

FIGURE 6
Time-variation curve of matric suction.

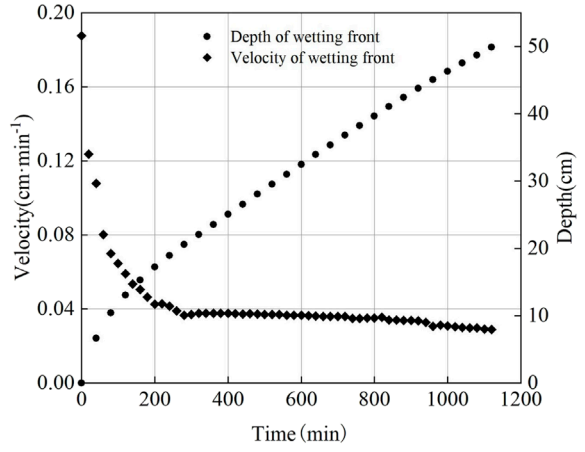

FIGURE 7
Time-varying curves of wetting front migration depth and migration velocity.

rate to less than 0.1 cm min^{-1}. As infiltration continued, the rate stabilized, approaching approximately 0.04 cm min^{-1}.

Numerical analysis of the seepage fields

Model establishment and selection of calculation conditions

Some undisturbed lateritic soils were taken for basic physical and mechanical tests in the laboratory to obtain the necessary calculation parameters for the simulation (Table 1).

A seepage calculation model was established via Geo-studio software on the basis of the geological section along the main sliding direction of the lateritic soil landslide. The model assumed an impermeable boundary at the base with a constant head of 1950 m on the left side and 1878 m on the right side. The slope surface was defined as a unit flux boundary to simulate rainfall infiltration, allowing for the subsequent design of rainfall intensity scenarios. Eight monitoring points were selected along the slope surface from top to bottom, and two characteristic profiles, 1–1′ and 2–2′, were chosen (Figure 8) to analyze changes during the seepage process. Considering the presence of favorable fracture pathways for rainfall infiltration in the actual slope, the permeability coefficient of the intact lateritic soil in the study area was increased by an order of magnitude to define the effective permeability coefficient of the red soil (Zhang, 2015). The soil-water characteristic curve was obtained via built-in sample functions within the software, and the experimental saturated permeability coefficient of the lateritic soil was fitted to the Fredlund and Xing model to derive the permeability coefficient function (Yu et al., 2017).

Calculation conditions

On the basis of the rainfall conditions in the study area, daily rainfall amounts of 24.9, 49.9, 99.9, and 249.9 mm were selected for subsequent analysis of the seepage characteristics of the lateritic soil slope. The rainfall duration was set to 2 days, followed by an 8-day rainless period. The calculation scenarios and load combinations are presented in Table 2.

Infiltration characteristics analysis

The process of rainfall infiltration caused the soil to transition from an unsaturated state to a saturated state. During this process, changes in the soil pore water pressure, moisture content, and matric suction occurred, which in turn affected the stability of the lateritic soil slope.

As shown in the time series curves of the pore water pressure on the slope surface (Figure 9), the monitoring points in the upper part of the slope were farther from the groundwater table, resulting in greater initial negative pore water pressure values. Conversely, the initial negative pore water pressure values at the slope toe were relatively low. As rainfall progressed, the upper slope experienced the greatest variation in pore water pressure, ranging from −467 kPa

TABLE 1 Calculation parameters.

Geotechnical category	Unit weight γ(kN·m3)	Cohesion c (kPa)	Internal friction angle Φ(°)	Saturated permeability coefficient k (cm·s−1)	Natural water content W (%)
Lateritic soil	19.5	21	13	1.7×10−5	28.8

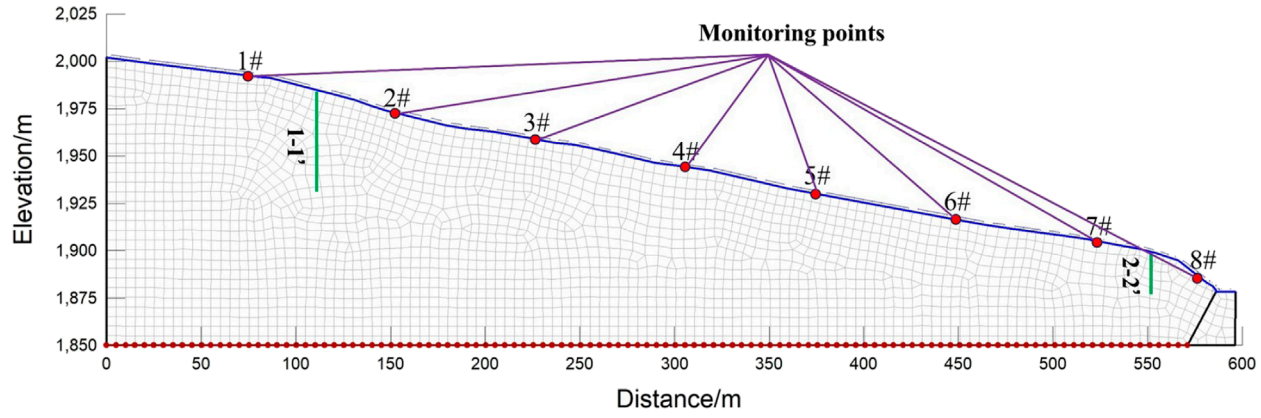

FIGURE 8
Layout of the model monitoring points and characteristic profiles.

TABLE 2 Table of calculation conditions and load combinations.

State	Id	Computational conditions	Load combinations
Normal state	1	Natural	Dead weight+Groundwater
Non-normal state	2	Continuous 2 days moderate rain	Dead weight+Groundwater+Moderate rain (Rainfall intensity:24.9 mm/d)
	3	Continuous 2 days heavy rain	Dead weight+Groundwater+Heavy rain (Rainfall intensity:49.9 mm/d)
	4	Continuous 2 days torrential rain	Dead weight+Groundwater+Torrential rain (Rainfall intensity:99.9 mm/d)
	5	Continuous 2 days downpour	Dead weight+Groundwater+Downpour (Rainfall intensity:249.9 mm/d)

to −30 kPa. With increasing rainfall intensity, the time required for each monitoring point to reach the peak pore water pressure decreased, and the rate of increase was greater in the upper slope than in the lower slope. The saturated permeability coefficient of the lateritic soil was lower than the rainfall intensity, meaning that the infiltration rate at later stages of rainfall was controlled by the permeability coefficient of the lateritic soil. After 2 days of rainfall at different intensities, the soil at the slope toe reached saturation, whereas the soil in the middle and upper parts of the slope remained in a nearly saturated state.

The spatial variation curves of pore water pressure under different rainfall intensities (Figures 10, 11) reveal that the primary changes in the seepage field during the entire rainfall process occurred in the shallow soil layers. A significant amount of rainfall infiltrated the slope surface, but owing to the fine particles and low permeability of the lateritic soil, the water could not migrate to deeper layers, resulting in a greater variation in pore water pressure in the shallow layers. As the rainfall intensity increased, the depth of influence also increased. In the upper part of the slope, the depth of influence was approximately 9–2 m, with little to no change in pore water pressure at greater depths as the rainfall intensity increased. In the lower part of the slope, the depth of influence was approximately 8–11 m, and deeper soil layers exhibited some fluctuations in pore water pressure with increasing rainfall intensity.

The pore water pressure variation trends at each monitoring point during the rainfall infiltration process were generally similar. Initially, the shallow soil layers in the slope gradually became saturated due to the influence of the rainfall infiltration rate. However, in the later stages, the low permeability coefficient of the lateritic soil impeded further infiltration, causing most of the rainfall to accumulate as surface runoff and discharge at the slope toe. After the rainfall ended, the low permeability of the lateritic soil

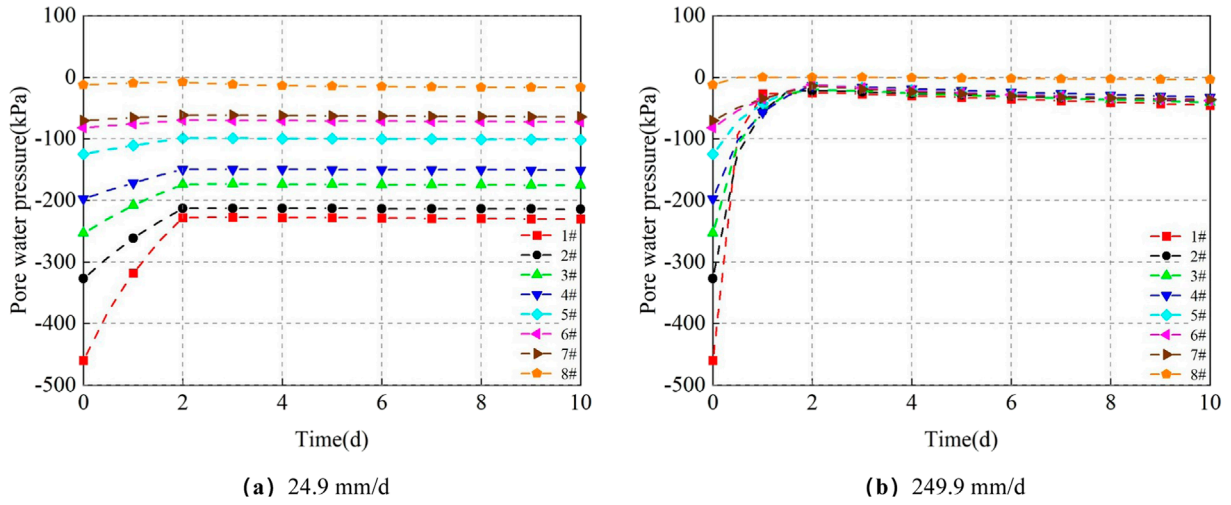

FIGURE 9
Time-variation curves of pore water pressure at slope monitoring points under different rainfall intensities. **(A)** 24.9 mm/d. **(B)** 249.9 mm/d.

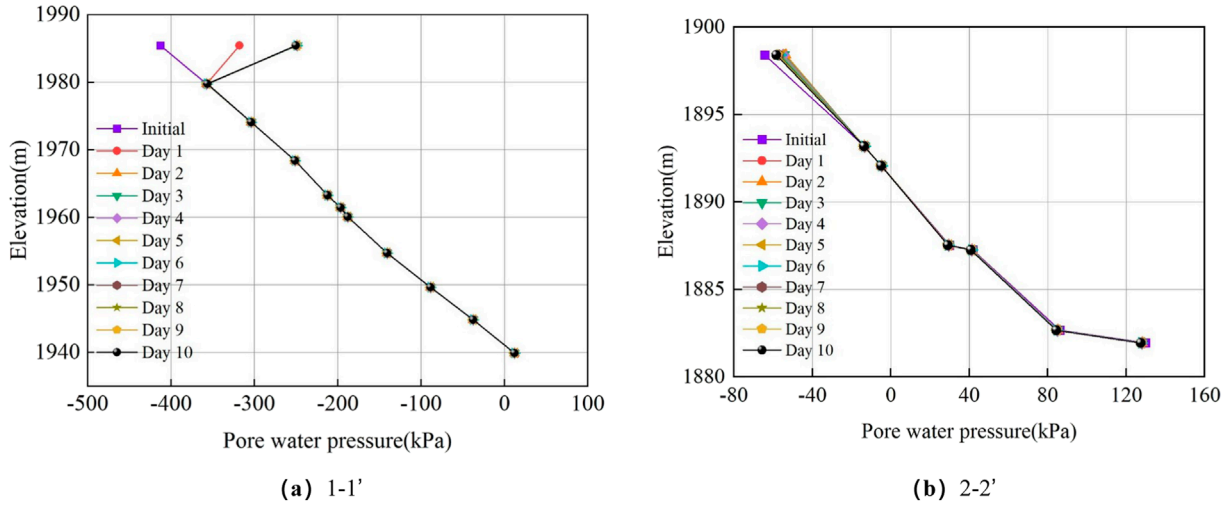

FIGURE 10
Elevation-variation curves of pore water pressure for different profiles under 24.9 mm/d rainfall intensity. **(A)** 1–1′. **(B)** 2–2′.

resulted in very slow water drainage, causing the pore water pressure at various points on the slope surface to remain near their peak values for an extended period, requiring a long time to return to the initial state.

As rainfall infiltrated from the shallow to deeper parts of the slope, the unsaturated zone gradually transitioned to a saturated zone. The pore water pressure variation was more significant in the middle and upper parts of the slope than in the lower part, whereas the deeper soil layers were less affected by rainfall, with minimal changes in pore pressure. Throughout the entire rainfall event, the saturation zone within the slope was confined to the shallow soil layers, where the matric suction decreased, leading to a reduction in soil strength. Stability calculations for the lateritic soil slope under different rainfall intensities indicate that, even after 2 days of rainfall, the landslide remained relatively stable. For the maximum rainfall intensity of 249.9 mm/d, the calculated stability factor of the landslide was 1.213.

Slope instability threshold study

Calculation scheme

The intensity and duration of rainfall are key factors determining whether instability occurs. To study the rainfall threshold for laterite slope instability, the rainfall intensity was gradually increased beyond the original level, without considering evaporation, to explore the stability of the laterite slope. Two calculation scenarios were designed: (1) Instability threshold under short-term heavy rainfall: the rainfall intensities were set at 400, 500, 600, 700, and

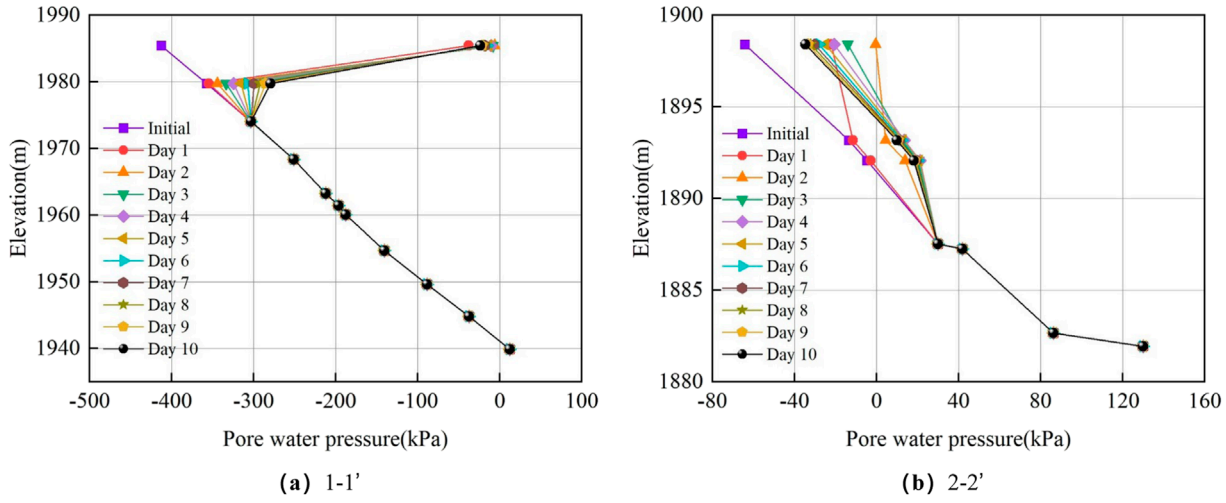

FIGURE 11
Elevation-variation curves of pore water pressure for different profiles under 249.9 mm/d rainfall intensity. **(A)** 1–1'. **(B)** 2–2'.

750 mm/d, with a rainfall duration of 2 days; (2) Instability threshold under long-term rainfall: the rainfall intensities were set at 50 mm/d for heavy rain, 100 mm/d for very heavy rain, and 120 mm/d for very heavy rain. Extensive data collection and surveys revealed that before the occurrence of large-scale landslides in Huili, Sichuan, the rainfall duration was often approximately 1 week. Therefore, in this study, the rainfall duration was set at 5 days to analyze the slope instability threshold under long-term rainfall.

Using the determined rainfall intensities, the stability coefficient of the lateritic soil slope was calculated via the Morgenstern–Price method in the SLOPE/W module. The local stability coefficients of the slope under rainfall intensities of 400, 500, 600, 700, and 750 mm/d were 1.188, 1.171, 1.088, 1.062, and 1.057, respectively.

Typically, when the slope stability factor falls below 1.05, deformation is likely to occur. Under a rainfall intensity of 750 mm/d, the slope stability factor approaches 1.05, indicating that this intensity is the threshold for instability under short-term intense rainfall conditions. However, an analysis of rainfall data from 1956 to 2022 revealed that the maximum single-day rainfall in the area over the past 66 years was 298.96 mm, indicating that it is unlikely that rainfall will reach the instability threshold under short-term intense rainfall conditions. Therefore, the lateritic soil landslide was not easily triggered by short-term intense rainfall, and subsequent analyses focused solely on seepage characteristics under long-term rainfall conditions.

Analysis of seepage characteristics under long-term rainfall conditions

Under rainfall intensities of 50, 100, and 120 mm/d, after 5 days of continuous rainfall followed by cessation, Figure 12 shows the variation curves of the volumetric water content at the slope surface monitoring points over time under rainfall intensities of 50 and 120 mm/d.

As shown in the figure, the volumetric water content at each monitoring point on the slope surface gradually increased with the continuation of rainfall, with the soil at the toe and crest of the slope reaching peak values first and the soil at the toe becoming saturated first. As the rainfall intensity increased, the rate of increase in the volumetric water content at each monitoring point accelerated. Overall, the rate of increase was as follows: upper slope > middle slope > lower slope. The time required for the monitoring points on the upper slope to reach peak values was significantly shorter, and after reaching the peak, the values stabilized. By the fifth day of rainfall, most monitoring points had reached peak values. Under a rainfall intensity of 120 mm/d, the soil at monitoring points 6# and 7# also approached saturation, indicating a significant rise in the groundwater level. After the rainfall ceased, moisture within the slope continued to migrate toward the toe, with the volumetric water content at the middle and upper monitoring points decreasing at the fastest rate. The water table retreated, with the volumetric water content at the monitoring point near the slope toe (7#) initially dropping sharply before stabilizing, while the soil at the toe remained saturated. Overall, even long time after the cessation of rainfall, the volumetric water content of the slope did not return to its initial state.

Figure 13 shows the variation in volumetric water content with elevation at the 2–2' profile near the slope toe under the two rainfall intensities of 50 and 120 mm/d. The figure indicates that the soil below the groundwater level was in a saturated state, whereas the range of volumetric water content variations in the shallow soil increased progressively with increasing rainfall intensity. The closer the soil was to the slope surface, the sooner it reached saturation. After the rainfall ended, the deeper the soil was, the slower the decrease in volumetric water content was.

A comparative analysis revealed that the slope toe was a vulnerable area. The greater the rainfall intensity was, the more water migrated toward the slope toe, continuously infiltrating and eroding the soil at the toe. This process gradually deteriorated the mechanical

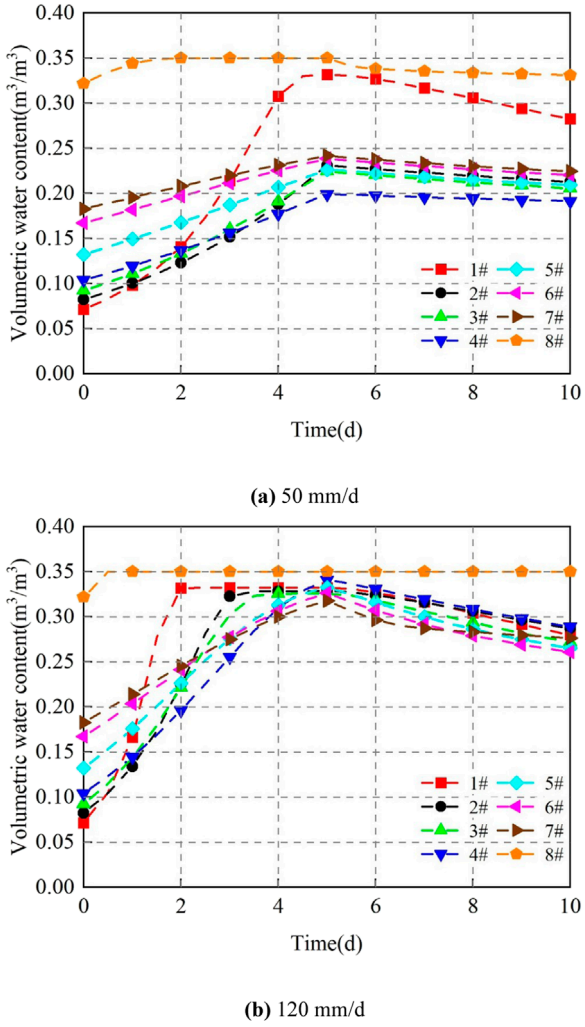

FIGURE 12
Time-variation curves of the volumetric water content at the slope monitoring points under the different rainfall intensities. **(A)** 50 mm/d. **(B)** 120 mm/d.

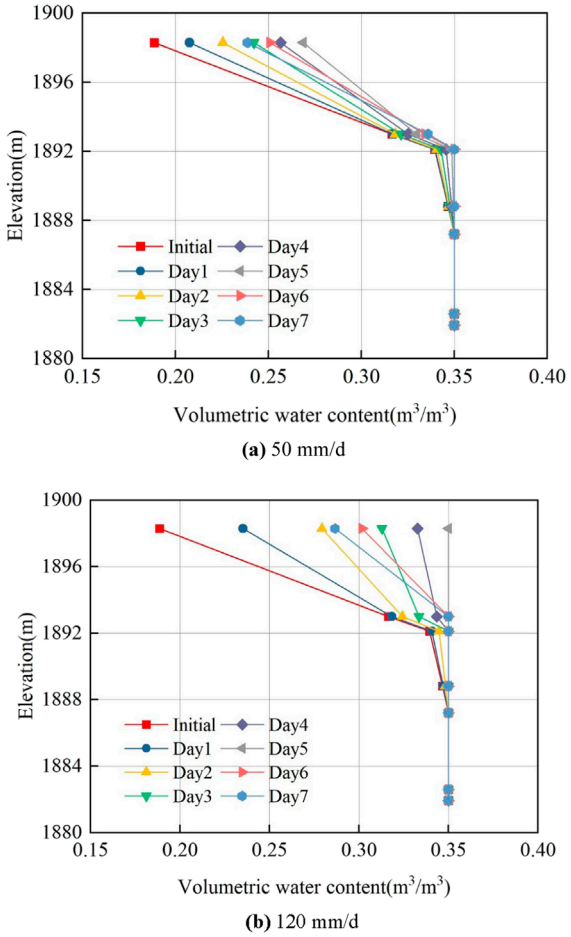

FIGURE 13
Elevation-variation curves of the volumetric water content for profile 2–2′ under the different rainfall intensities. **(A)** 50 mm/d. **(B)** 120 mm/d.

properties of the soil, leading to a reduction in its strength and, consequently, a decrease in slope stability.

Rainfall threshold analysis

The local stability characteristics of the lateritic soil slope under long-term rainfall conditions were as follows: In a continuous 5-day rainfall environment, the stability coefficient was 1.210 when the rainfall intensity was 50 mm/day, 1.171 when the rainfall intensity was 100 mm/day, and 1.049 when the rainfall intensity was 120 mm/day. When the rainfall intensity was 120 mm/day and it rained continuously for 5 days, the local stability of the lateritic soil slope approached 1.05. This rainfall intensity can be regarded as the threshold for slope instability under prolonged rainfall conditions. The curve of the stability coefficient of the lateritic soil slope over time under a rainfall intensity of 120 mm/day is shown in Figure 14.

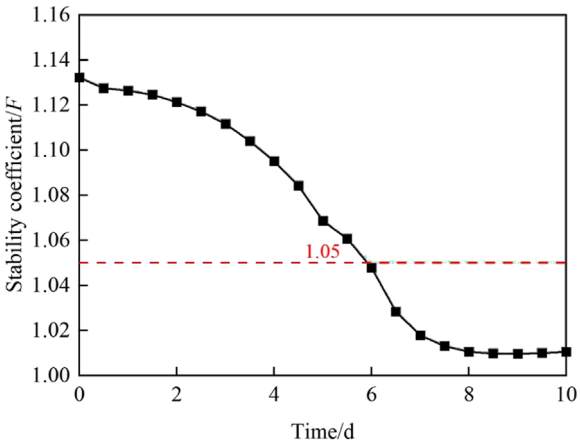

FIGURE 14
Time-variation curves of the slope stability coefficient under a 120 mm/d rainfall intensity.

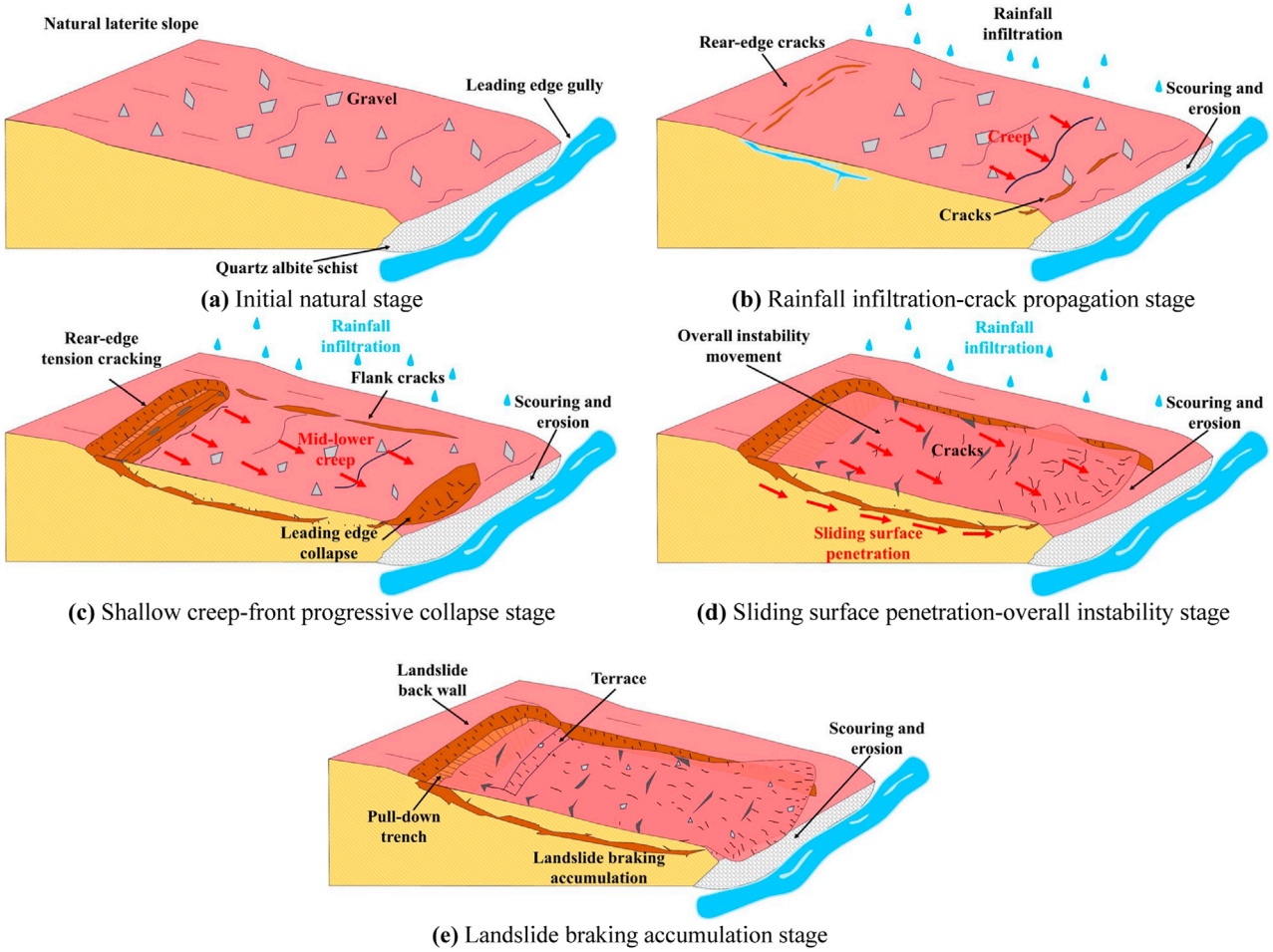

FIGURE 15
Formation stages of the lateritic soil landslide. **(A)** Initial natural stage. **(B)** Rainfall infiltration-crack propagation stage. **(C)** Intensified Shallow creep-front progressive collapse stage. **(D)** Sliding surface penetration-overall instability stage. **(E)** Landslide braking accumulation stage.

The study area experiences an average of 127 rainy days per year, with a maximum of 192 days. Rain occurs in almost one-third of the year, and in the wettest years, rain can occur up to half of the year. However, owing to the lack of detailed rainfall data, continuous rainfall for 5 days or more is possible in years with a high number of rainy days. Additionally, a continuous rainfall intensity exceeding 100 mm/day and even surpassing 120 mm/day can occur. On the basis of the analysis of a large amount of landslide data and investigations, large-scale landslides in the study area tend to form after approximately 5 days of heavy rainfall. Under long-term rainfall conditions, the instability threshold of slopes is approximately 120 mm/day.

Comprehensive analysis of slope instability and failure

The slope where the lateritic soil landslide occurs possesses both internal and external factors favorable for landslide occurrence. Rainfall and water erosion weaken the strength of the soil at the slope front edge, causing destabilization and removal of the front soil by water flow. This process continually pulled down the lateritic soil, ultimately leading to the formation of the landslide. On the basis of actual geological field investigations, combined with indoor physical and mechanical tests, rainfall infiltration tests, and slope seepage simulations, the formation process of this landslide can be divided into five stages, as shown in Figure 15.

(1) Initial natural stage (Figure 15A): In this stage, the soil in the shallow range of the lateritic soil slope was in full contact with the air and underwent intense physical and chemical weathering. The soil exhibited reddish-brown and yellow-brown hues, with the surface layer being relatively loose under natural conditions. Randomly developed cracks of varying degrees are present within the soil.

(2) Rainfall infiltration and crack expansion stage (Figure 15B): The front part of the slope was steeper, while the middle and rear sections formed a platform. The continuous scouring of the front edge by flowing water led to further steepening of the slope, improving free-face conditions. After long-term rainfall, the slope exhibited a tendency for downward creeping, and tensile cracks gradually develop in the middle and rear

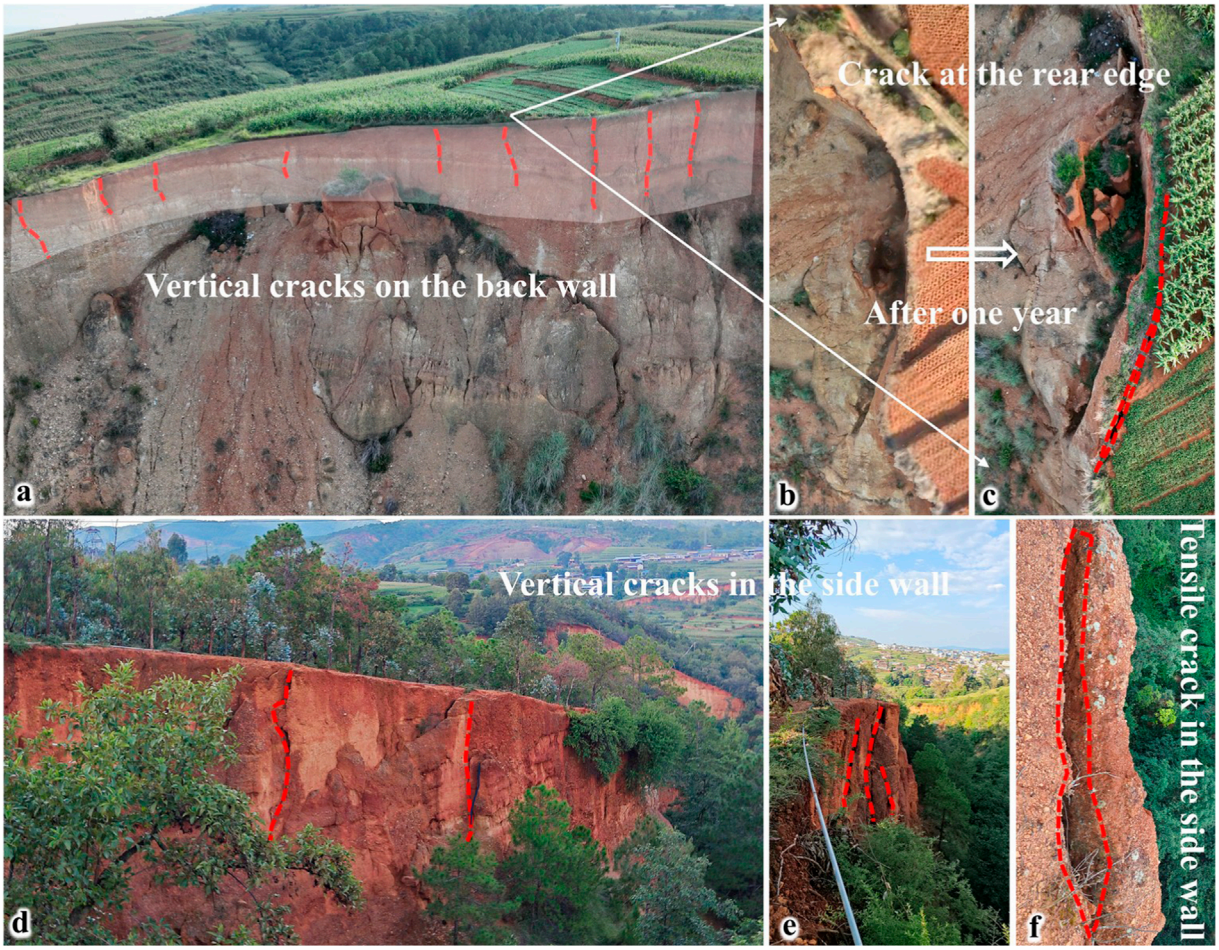

FIGURE 16
Spatial variability characteristics of the lateritic soil in the study area **(A)**. Vertical cracks on the back wall; **(B, C)**. Crack at the rear edge; **(D, E)** vertical cracks in the side wall; **(F)** tensile crack in the side wall).

sections. Rainwater infiltrated through these preferentially developed cracks, softening the soil around the cracks and reducing its shear strength. Additionally, the flowing water exerted hydrodynamic pressure on the cracks, causing further crack propagation under prolonged rainfall.

(3) Intensified shallow sreep and progressive collapse of the front slope (Figure 15C): Under continued rainfall, the expansion of shallow cracks accelerated water infiltration, altering the slope's seepage field and facilitating water migration to the middle and lower parts of the slope. The shallow slope body experienced increased creep movement. Crack propagation in the rear section formed the rear boundary of the potential landslide, and a sliding surface gradually developed. Due to the low permeability of the lateritic soil, rainwater accumulated and flowed toward the slope toe. Combined with fluvial scouring and erosion, this caused a reduction in the shear strength of the local soil at the slope's front, leading to progressive collapse in localized areas.

(4) Sliding surface penetration and overall instability stage (Figure 15D): The local collapse of the front slope enhanced free-face conditions, further exacerbating the pulling effect on the rear slope. The landslide involved a larger planar area, located in a surface water collection and runoff zone. With continued rainwater infiltration, the slope undergone progressive downslope creep, and the cracks along the lateral boundaries and the potential sliding surface gradually connected, resulting in overall slope failure. Portions of the front slope's material accumulate at the base.

(5) Landslide braking and accumulation stage (Figure 15E): During the landslide, the different sliding speeds of the upper and lower sections formed landslide terraces in the upper part. The sliding mass overcame sliding resistance, dissipated kinetic energy, and the front sliding mass spread and accumulated to the sides. The overall sliding distance was short, and the sliding speed gradually decreased to zero. The landslide gradually stabilized, eventually forming the current lateritic soil landslide.

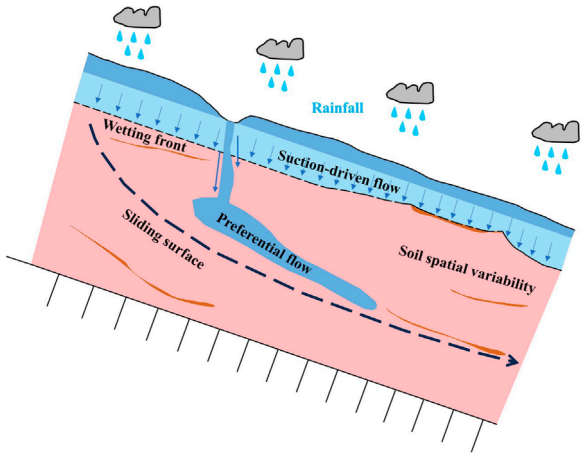

FIGURE 17
Schematic diagram of preferential flow pathways (modified from Ma et al., 2024).

Discussion

This study analyzed the seepage characteristics and stability changes of the lateritic landslide under rainfall conditions. Based on existing rainfall data, two simplified uniform rainfall patterns were considered: short-term intense rainfall and long-term rainfall. In reality, rainfall data vary continuously over time and space, making accurate measurement difficult. Therefore, variations in rainfall are often neglected in slope stability analyses (Ruette et al., 2014). Most previous studies have focused on the effects of rainfall intensity and duration on the stability of unsaturated slopes (Jeong et al., 2017; Liu et al., 2023). However, rainfall in a given region is not always uniform, and various combinations of rainfall patterns can occur. Different rainfall patterns can alter the boundary conditions of slopes and influence water movement within the slope, particularly with prolonged rainfall, which allows for buffering time during the infiltration process, leading to a continuous decrease in matric suction within the slope (Tsai and Wang, 2011). Ma et al. (2024) investigated the impact of rainfall patterns on the stability of loess slopes and found that using a uniform rainfall pattern for slope stability analysis tends to yield conservative results. Additionally, they validated their findings with rainfall and landslide data from similar regions (Luo et al., 2023; Wang et al., 2022; Shao et al., 2023; Zhuang et al., 2018), indicating that landslide instability often occurs during continuous rainfall or when heavy rain follows preceding rainfall events. The conclusion that the old lateritic landslide in the study area resulted from long-term rainfall aligns with these findings.

Moreover, during the numerical analysis using Geo-studio software, the soil is assumed to be homogeneous, with constant values for soil parameters. The determination of these parameters is subject to uncertainties and requires parameter inversion to obtain final values. Due to variations in geological processes and changing climatic conditions, the pore structure of natural soils exhibits temporal and spatial variability, leading to uncertainties in soil hydraulic parameters, which may reduce the overall stability of slopes. Li et al. (2023a) highlighted that soil heterogeneity can influence the infiltration process within soil slopes, as well as the post-rainfall stability and failure timing of the slopes. In the study area, cracks and vertical joints were observed in certain regions of the lateritic soil (Figure 16), similar to those found in loess (Zhao et al., 2020; Feng et al., 2020). These features can form preferential pathways for water infiltration. During the infiltration process, the uneven distribution of water can result in heterogeneity in infiltration rates, matric suction, and pore water pressure changes. Figure 17 illustrates the concept of water infiltration in slopes with preferential pathways and spatial variability of soil properties.

Conclusion

Taking a lateritic soil landslide in Yunnan Province as the research object, the slope seepage characteristics were analyzed through seepage and stability coupling. Two schemes, short-term heavy rainfall and prolonged rainfall, were designed to analyze the instability threshold of the slope, leading to the following conclusions:

(1) During water infiltration, the infiltration time curve of the lateritic soil column shows a parabolic growth trend. The migration rate of the wetting front rapidly decreased from 0.15 to 0.2 cm/min to 0.1 cm/min and then stabilized at approximately 0.04 cm/min.
(2) Long-term rainfall is the inducing condition for the formation of this lateritic soil landslide. Considering the changes in the stability of the lateritic soil slope under different rainfall conditions, the instability threshold of the slope under 5 days of prolonged rainfall is approximately 120 mm/day.
(3) Due to the low permeability of lateritic soil, the main changes in the seepage field during rainfall occurred in the shallow soil layer. In the later stages of rainfall, the infiltration rate of the slope was controlled by the permeability coefficient of the lateritic soil. As the rainfall intensity increased, the depth of rainfall impact increased, and the pore water pressure in the shallow soil layer tended to gradually increase and then stabilize under different rainfall intensities.
(4) Under long-term rainfall conditions, the volumetric water content of the soil at the toe of the lateritic soil slope first peaked. After the rainfall ends, the moisture in the slope continues to migrate to the toe, keeping the soil at the toe in a saturated state.
(5) Comprehensive analysis divided the formation process of this lateritic soil landslide into five stages: initial natural stage, rainfall infiltration-crack expansion, shallow creep-progressive collapse of the front edge, sliding surface penetration-overall instability, and landslide braking and accumulation.

Data availability statement

The original contributions presented in the study are included in the article/supplementary material, further inquiries can be directed to the corresponding author.

Ethics statement

Written informed consent was obtained from the individual(s) for the publication of any potentially identifiable images or data included in this article.

Author contributions

CG: Data curation, Formal Analysis, Investigation, Methodology, Project administration, Resources, Software, Supervision, Validation, Visualization, Writing–original draft, Writing–review and editing. LC: Writing–review and editing. WZ: Writing–review and editing. WL: Writing–review and editing. HM: Conceptualization, Data curation, Writing–original draft, Writing–review and editing. HL: Writing–original draft, Writing–review and editing. FJ: Conceptualization, Formal Analysis, Funding acquisition, Investigation, Methodology, Project administration, Resources, Software, Supervision, Validation, Visualization, Writing–review and editing.

Funding

The author(s) declare that financial support was received for the research, authorship, and/or publication of this article. This study was financially supported by the Foundation of the National Natural Science Foundation of China (Grant No. 41977237).

Acknowledgments

We greatly appreciate editors and reviewers for their critical comments and suggestions. Their constructive comments are of great help to improve the quality of this paper.

Conflict of interest

Authors CG, LC, and WZ were employed by Liangshan Mining Co., Ltd.

The remaining authors declare that the research was conducted in the absence of any commercial or financial relationships that could be construed as a potential conflict of interest.

Publisher's note

All claims expressed in this article are solely those of the authors and do not necessarily represent those of their affiliated organizations, or those of the publisher, the editors and the reviewers. Any product that may be evaluated in this article, or claim that may be made by its manufacturer, is not guaranteed or endorsed by the publisher.

References

Bai, W. S., Li, R. J., Pan, J. Y., Li, R. J., Wang, L., and Yang, Z. W. (2023). Measured rainfall infiltration and the infiltration interface effect on double-layer loess slope. *Water* 15 (14), 2505. doi:10.3390/w15142505

Bhavithra, S., Senthilkumar, V. S., and Sembulichampalayam, C. (2024). Investigation of rainfall-induced landslide on unsaturated lateritic residual soil slope in Nilgiris, Western Ghats, India using deterministic and reliability analysis. *Bull. Eng. Geol. Environ.* 83 (6), 1–19. doi:10.1007/s10064-024-03704-y

Chantruthai, P., Areepong, T., Issaro, S., and Jaritngam, S. (2017). Investigating lateritic soil properties and impacts from quarrying activity on communities in southern Thailand: a case study. *Eng. J.* 21 (1), 265–278. doi:10.4186/ej.2017.21.1.265

Chen, K. S. (2014). Artificial rainfall failure experiments for a red clay slope. *Appl. Mech. and Mat.* 638-640, 402–406. doi:10.4028/www.scientific.net/AMM.638-640.402

Cheng, H., Wu, Z. J., Chen, H., and Zhou, X. P. (2024). Stability analysis of unsaturated-saturated soil slopes under rainfall infiltration using the rigorous limit equilibrium method. *Bull. Eng. Geol. Environ.* 83 (4), 147–222. doi:10.1007/s10064-024-03623-y

Cui, W., Yang, J., and Liu, L. (2007). Analysis of continuous rainfall conditions on stability of unsaturated soil slope. *Hydrogeol. Eng. Geol.* 34 (3), 55–58. doi:10.3969/j.issn.1000-3665.2007.03.014

Feng, L., Lin, H., Zhang, M. S., Li, G., Jin, Z., and Liu, X. B. (2020). Development and evolution of Loess vertical joints on the Chinese Loess Plateau at different spatiotemporal scales. *Eng. Geol.* 265, 105372. doi:10.1016/j.enggeo.2019.105372

Fourie, A. B., Rowe, D., and Blight, G. E. (1999). The effect of inÆltration on the stability of the slopes of a dry ash dump. *Geotechnique* 49 (1), 1–13. doi:10.1680/geot.1999.49.1.1

Froude, M. J., and Petley, D. N. (2018). Global fatal landslide occurrence from 2004 to 2016. *Nat. Hazards. Earth Syst. Sci.* 18 (8), 2161–2181. doi:10.5194/nhess-18-2161-2018

Fu, B. C., Huang, Y., and Fang, L. P. (1997). Lateritization and engineering geology classlfication of laterite. *Yunnan Geol.* (2), 197–206. CNKI:SUN:YNZD.0.1997-02-008.

Fu, H. Y., Zeng, L., Jiang, Z. M., and He, Z. M. (2012). Developing law of transient saturated areas of highway slope under rainfall conditions. *China J. Highw. Transp.* 25 (3), 59–64. doi:10.19721/j.cnki.1001-7372.2012.03.004

Gong, Q. B., Yin, K. L., Xiao, C. G., Chen, L. X., Yan, L. X., Zeng, T. R., et al. (2024). Double-index model of landslide meteorological warning based on the I-D threshold. *Bull. Geol. Sci. Technol.* 43 (01), 262–274. doi:10.19509/j.cnki.dzkq.tb20220254

Hou, T. S., Duan, X., and Liu, H. Y. (2021). Study on stability of exit slope of Chenjiapo tunnel under condition of long-term rainfall. *Environ. Earth Sci.* 80 (17), 590–614. doi:10.1007/s12665-021-09895-x

Jeong, S., Lee, K., Kim, J., and Kim, Y. (2017). Analysis of rainfall-induced landslide on unsaturated soil slopes. *Sustainability* 9(7), 1280. doi:10.3390/su9071280

Li, L. J., Jian, W. X., Zhang, D. M., Dong, Z. H., Zhang, B., and Pan, Y. L. (2021). Seepage characteristics and stability of Tanjiawan cccumulation landslide with cracks under rainstorm. *Saf. Environ. Eng.* 28 (01), 135–143. doi:10.13578/j.cnki.issn.1671-1556.2021.01.019

Li, X. Y., Liu, X., Liu, Y. D., Yang, Z. Y., and Zhang, L. M. (2023a). Probabilistic slope stability analysis considering the non-stationary and spatially variable permeability under rainfall infiltration-redistribution. *Bull. Eng. Geol. Environ.* 82, 350. doi:10.1007/s10064-023-03351-9

Li, Y., Xue, K. X., Zhao, Y., Wang, C. L., Bi, J., Wang, T. Y., et al. (2023b). Study on the stability and disaster mechanism of layered soil slopes under heavy rain. *Bull. Eng. Geol. Environ.* 82 (7), 272–323. doi:10.1007/s10064-023-03277-2

Liu, X., Wang, Y., and Leung, A. K. (2023). Numerical investigation of rainfall intensity and duration control of rainfall-induced landslide at a specific slope using slope case histories and actual rainfall records. *Bull. Eng. Geol. Environ.* 82 (8), 333–420. doi:10.1007/s10064-023-03359-1

Liu, Z. Z., Yan, Z. X., Peng, N. B., Duan, J., and Ren, Z. H. (2012). Dynamic influence of sustained small-rainfall infiltration on stability of unsaturated soil slope. *J. Civ. Archit. Environ. Eng.* 34 (4), 19–23. doi:10.3969/j.issn.1674-4764.2012.04.004

Lu, X. S., Jiang, Y., Wang, N. Q., and Shen, H. H. (2023). Progressive deformation and failure mechanism of loess fill slopes induce by rainfall: insights from flume model tests. *Bull. Eng. Geol. Environ.* 82 (10), 385–418. doi:10.1007/s10064-023-03413-y

Luo, L., Guo, W. Z., Tian, P., Liu, Y. L., Wang, K. S., and Luo, J. W. (2023). Unique landslides (loess slide-flows) induced by an extreme rainstorm in 2018 on the Loess Plateau: a new geological hazard and erosion process. *Int. J. Sediment. Res.* 38 (2), 228–239. doi:10.1016/j.ijsrc.2022.07.009

Ma, B. Q., Du, Y. P., Wang, H. X., Yang, A. Q., Wang, X. D., and Tian, K. L. (2021). Experimental study on stability of loess slope stability under continuous rainfall. *J. Soil Water Conserv.* 35 (5), 50–56. doi:10.13870/j.cnki.stbcxb.2021.05.008

Ma, J. H., Yao, Y. Q., Wei, Z. R., Meng, X. M., Zhang, Z. L., Yin, H. L., et al. (2024). Stability analysis of a loess landslide considering rainfall patterns and spatial variability of soil. *Comput. Geotech.* 167. 106059. doi:10.1016/j.compgeo.2023.106059

Ruette, J. V., Lehmann, P. D., and Or, D. (2014). Effects of rainfall spatial variability and intermittency on shallow landslide triggering patterns at a catchment scale. *Water Resour. Res.* 50 (10), 7780–7799. doi:10.1002/2013WR015122

Sani, Y. H., and Eisazadeh, A. (2023). Influence of coir fiber on the strength and permeability characteristics of bottom ash- and lime-stabilized laterite soil. *Int. J. Geosynth. Ground Eng.* 9 (5), 63–15. doi:10.1007/s40891-023-00483-6

Shao, X. Y., Ma, S. Y., Xu, C., and Xu, Y. R. (2023). Insight into the characteristics and triggers of loess landslides during the 2013 heavy rainfall event in the Tianshui area. China. *Remote Sens.* 15 (17), 4304. doi:10.3390/rs15174304

Shi, Z. M., Shen, D. Y., Peng, M., Zhang, L. L., Zhang, F. W., and Zheng, X. Z. (2016). Slope stability analysis by considering rainfall infiltration in multi-layered unsaturated soils. *J. Hydraul. Eng.* 47 (8), 977–985. doi:10.13243/j.cnki.slxb.20151132

Song, X. H., Tan, Y., and Zhang, S. J. (2021). Investigation on effects of vegetations on stability of sandy slope by indoor rainfall model test. *J. Harbin Inst. Technol.* 53 (5), 123–133. doi:10.11918/201908166

Sun, Y., Wei, W., Wang, B. L., and Li, H. J. (2022). Study on monitoring and early warning of landslide hazard under rainfall——taking Sunning Chuanshan as an Example. *J. Catastrophol.* 37 (04), 64–68. doi:10.3969/j.issn.1000-811X.2022.04.011

Sun, Y., Zhang, J., Wang, H., and Lu, D. G. (2024). Probabilistic thresholds for regional rainfall induced landslides. *Comput. Geotech.* 166, 106040. doi:10.1016/j.compgeo.2023.106040

Tao, G. L., Feng, S. J., Xiao, H. L., Gu, K., and Wu, Z. J. (2024). Rainfall infiltration test and numerical simulation analysis of a large unsaturated soil slope. *J. Hydrol. Eng.* 29 (4). doi:10.1061/JHYEFF.HEENG-6190

Tran, T. V., Alvioli, M., Lee, G., and An, H. U. (2018). Three-dimensional, time-dependent modeling of rainfall-induced landslides over a digital landscape: a case study. *Landslides* 15 (6), 1071–1084. doi:10.1007/s10346-017-0931-7

Tsai, T. L., and Wang, J. K. (2011). Examination of influences of rainfall patterns on shallow landslides due to dissipation of matric suction. *Environ. Earth Sci.* 63, 65–75. doi:10.1007/s12665-010-0669-1

Wang, H. J., Sun, P., Zhang, S., Ren, J., Wang, T., and Xin, P. (2022). Evolutionary and dynamic processes of the zhongzhai landslide reactivated on october 5, 2021, in niangniangba, gansu province. China. *Landslides*. 19, 2983–2996. doi:10.1007/s10346-022-01966-9

Wang, L., Wu, C. Z., Li, Y. Q., Liu, H. L., Zhang, W. W., and Chen, X. (2019). Probabilistic risk assessment of unsaturated slope failure considering spatial variability of hydraulic parameters. *KSCE. J. Civ. Eng.* 23 (12), 5032–5040. doi:10.1007/s12205-019-0884-6

Xu, J. W., Ueda, K., and Uzuoka, R. (2022). Numerical modeling of seepage and deformation of unsaturated slope subjected to post-earthquake rainfall. *Comput. Geotech.* 148, 104791. doi:10.1016/j.compgeo.2022.104791

Ye, L. Z., Liu, K., and Huang, Y. Y. (2015). Analysis on action mode and prevention of landslide groundwater in Fujian Province. *Geol. Rev.* 61 (S1), 55–56.

Yu, S. Y., Zhang, J. X., Wang, J. L., Wang, T. X., Zhu, W. W., and Hu, N. X. (2017). Seepage and slope stability analysis under different rainfall patterns based on Fredlund&Xing parameters. *J. China Three Gorges Univ.(Nat. Sci.)* 39 (06), 46–51. doi:10.13393/j.cnki.issn.1672-948X.2017.06.010

Yuan, B. X., Cai, Z. R., Lu, M. M., Lv, J. B., Su, Z. L., and Zhao, Z. Q. (2020). Seepage analysis on the surface layer of multistage filled slope with rainfall infiltration. *Adv. Civ. Eng.* 2020. doi:10.1155/2020/8879295

Zeng, L., Shi, Z. M., Fu, H. Y., and Bian, H. B. (2017). Influence of rainfall infiltration on distribution characteristics of slope transient saturated zone. *China J. Highw. Transp.* 30 (1), 25–34. doi:10.19721/j.cnki.1001-7372.2017.01.004

Zhang, Q. 2015. *Study on the development and distribution characteristicsand early warning of slow-inclination shallow soil landslidesin red bed areainduced by rainfall-in Sichuan Nanjiang, for example*.

Zhao, K. Y., Xu, Q., Liu, F. Z., Zhang, X. L., and Ren, X. (2020). Field monitoring of preferential infiltration in loess using time-lapse electrical resistivity tomography. *J. Hydrol.* 591, 125278. doi:10.1016/j.jhydrol.2020.125278

Zheng, K. H., Luo, Z. Q., Luo, C. Y., and Wen, L. (2016). Layered gravel soil slope stability of a waste dump considering long-term hard rain. *Chin. J. Eng.* 38 (9), 1204–1211. doi:10.13374/j.issn2095-9389.2016.09.002

Zhou, Y. L., He, Q., Li, M., Sun, Z. Y., and He, F. H. (2023). Stability analysis of unsaturated soil slope considering seepage-stress coupling under different rainfall conditions. *J. Chongqing Jiaot. Univ. (Nat.l Sci.)* 42 (08), 57–63. doi:10.3969/j.issn.1674-0696.2023.08.09

Zhuang, J. Q., Peng, J. B., Wang, G. H., Javed, I., Wang, Y., and Li, W. (2018). Distribution and characteristics of landslide in Loess Plateau: a case study in Shaanxi province. *Eng. Geol.* 236, 89–96. doi:10.1016/j.enggeo.2017.03.001